

Ground test characterization of the Multiband Imaging Photometer for SIRTf (MIPS)

Erick T. Young^{*a}, George H. Rieke^a, James D. Cadien^a, Hervé A. Dole^a, Charles W. Englebracht^a,
Karl D. Gordon^a, Gerald B. Heim^b, Douglas M. Kelly^a, and John A. Stansberry^a
^aSteward Observatory/The University of Arizona; ^bBall Aerospace & Technologies Corp.

ABSTRACT

We describe the ground testing and characterization of the Multiband Imaging Photometer for SIRTf (MIPS). This instrument is a camera with three focal plane arrays covering broad spectral bands centered at 24 μm , 70 μm , and 160 μm . The instrument features a variety of operation modes that permit accurate photometry, diffraction-limited imaging, efficient mapping, and low resolution spectral energy distribution determinations. The observational philosophy of MIPS relies heavily on the frequent use of internal relative calibration sources as well as a high level of redundancy in the data collection. We show that by using this approach, users of MIPS can expect very sensitive, highly repeatable observations of astronomical sources. The ground characterization program for MIPS involved a number of facilities including test dewars for focal-plane level testing, a specialized cryostat for instrument-level testing, and tests in the flight SIRTf Cryo-Telescope Assembly.

Keywords: SIRTf, infrared, astronomy, photometry, MIPS

1. INTRODUCTION

The Space Infrared Telescope Facility (SIRTf) will be the final installment in NASA's series of Great Observatories. SIRTf is an 85-cm cryogenically cooled telescope with instrumentation that spans wavelengths between 3 μm to 160 μm . Despite its small size, SIRTf will provide unprecedented sensitivity at these wavelengths thanks to the combination of excellent observing conditions, cold optics, and advanced infrared detector arrays. SIRTf will be launched in early 2003 and has an anticipated lifetime between 2.5 and 5 years.

The Multiband Imaging Photometer for SIRTf (MIPS)¹ is one of the three science instruments on SIRTf. The Infrared Array Camera (IRAC)² provides imaging in four bands at 3.6, 4.5, 5.8, and 8.0 μm . The Infrared Spectrograph (IRS)³ produces low and moderate resolution spectra from 4 to 40 μm . MIPS provides imaging in three broad photometric bands centered at 24 μm , 70 μm , and 160 μm . The three bands view adjacent regions of the sky simultaneously. A number of design principles guided the development of MIPS. First, the performance of the instrument was to be limited only by natural backgrounds. Hence, attaining excellent detector sensitivity with good photometric behavior was required. Second, we felt that the greatest gains over previous missions were to come from significantly larger focal plane arrays. The desire for large formats led to the development of the largest far infrared array ever built. Third, simplicity and reliability were essential. Hence, MIPS has a minimum number of cryogenic mechanisms and no filter wheel. The single mechanism is a scan mirror, derived from a design used on the Infrared Space Observatory. This scan mechanism was included to perform the essential function of source modulation on the detector, but it is also used for beam switching and scanning.

2. OBSERVING MODES

To support the wide range of potential scientific investigations, MIPS offers a number of different operating modes. Precision photometry of compact sources is accomplished with the Photometry Mode. Here the source is repeatedly modulated on various parts of the detector arrays using the scan mirror. In this way, a highly redundant image of a small part of sky is built up. To survey large areas, MIPS has the Scan Map Mode. This mapping is accomplished by slowly scanning the telescope and "freezing" the motion by moving the internal scan mirror at a synchronized rate. In this way, the long settling time for the facility normally required to step from point to point is avoided. Besides imaging, MIPS can also be used to measure low-resolution ($\lambda / \Delta\lambda \sim 20$) spectral energy distributions between 50 and 95 μm using the

* eyoung@as.arizona.edu; phone 520-621-4119; fax 520-621-9555; Steward Observatory, University of Arizona, 933 N Cherry Ave, Tucson AZ 85721.

Spectral Energy Distribution Mode. Finally, MIPS provides a Total Power mode where part of the 70 μm field of view is modulated between the sky and a dark portion of the instrument interior.

3. DETECTORS

To cover the wide wavelength range, MIPS uses three very different focal plane technologies. Their characteristics are summarized in Table 1. The 24 μm band uses a 128x128 pixel Si:As Blocked Impurity Band (BIB) detector manufactured by Boeing North America. The extrinsic silicon detector material is indium bump bonded to a matching silicon readout that provides an amplifier per pixel and multiplexes the image data onto four output lines. The silicon BIB technology is mature, and detectors of excellent performance have been produced. Because of the special BIB construction of the detectors, the devices show excellent photometric characteristics and immunity from many radiation effects. The 24 μm focal plane array is mounted on a thermally isolated fixture that allows operation of the array at the optimum 6 K temperature (Figure 1). The mount also incorporates approximately 1 cm of aluminum shielding to minimize total dose of ionizing radiation. The

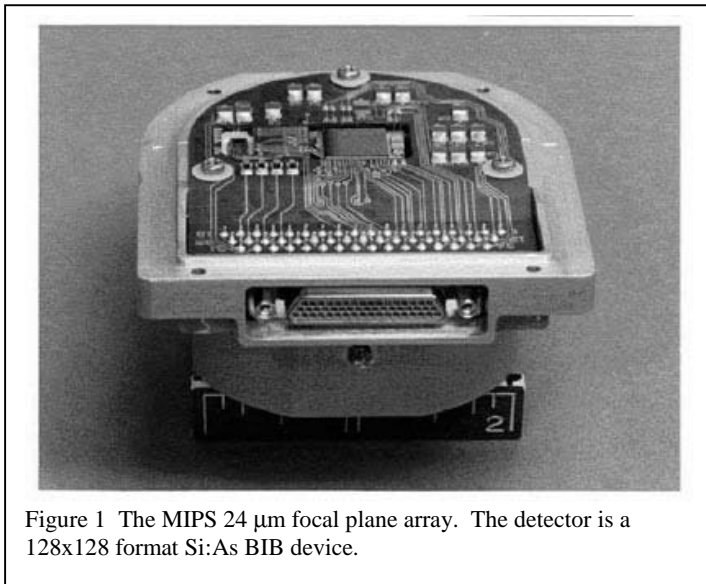


Figure 1 The MIPS 24 μm focal plane array. The detector is a 128x128 format Si:As BIB device.

The development of the Boeing Si:As arrays for SIRTf was led by the Infrared Spectrograph (IRS) team; that instrument uses identical arrays for two of the spectrograph modules. These detectors have been discussed by Van Cleve et al⁴.

Table 1. Characteristics of MIPS Focal Plane Arrays

Property	24 μm	70 μm	160 μm
Format	128x128	32x32	2x20 1 Pixel gap between rows
Detector	Si:As BIB	Ge:Ga	Stressed Ge:Ga
Wavelength Coverage	21.6-26.4 μm	50 – 80 μm	142-178 μm
Pixel Physical Size	75 μm	750 μm	3 mm (cone input)
Pixel Field of View	2.5" x 2.5"	9.8" x 9.8" or 5.0" x 5.0"	16"
Array Field of View	5.4' x 5.4'	5.2' x 5.2' or 2.7' x 2.7'	5.3' x 0.8' (with 1 row gap)
Supplier	Boeing North America	University of Arizona	University of Arizona
Readout	Source Follower	CRC-696 CTIA	CRC-696 CTIA
Dark Current	3 e ⁻ /s	150 e ⁻ /s	500 e ⁻ /s
Read Noise	27 e ⁻	92 e ⁻	250 e ⁻
Responsivity	53% (ηG @ 11.6 μm)	6.9 A/W	13 A/W
Detective Quantum Efficiency	52% @ 11.6 μm	18%	15%
Full Well Capacity	200,000 e ⁻	314,000 e ⁻	316,000 e ⁻
Operability	99.94%	98%	100%

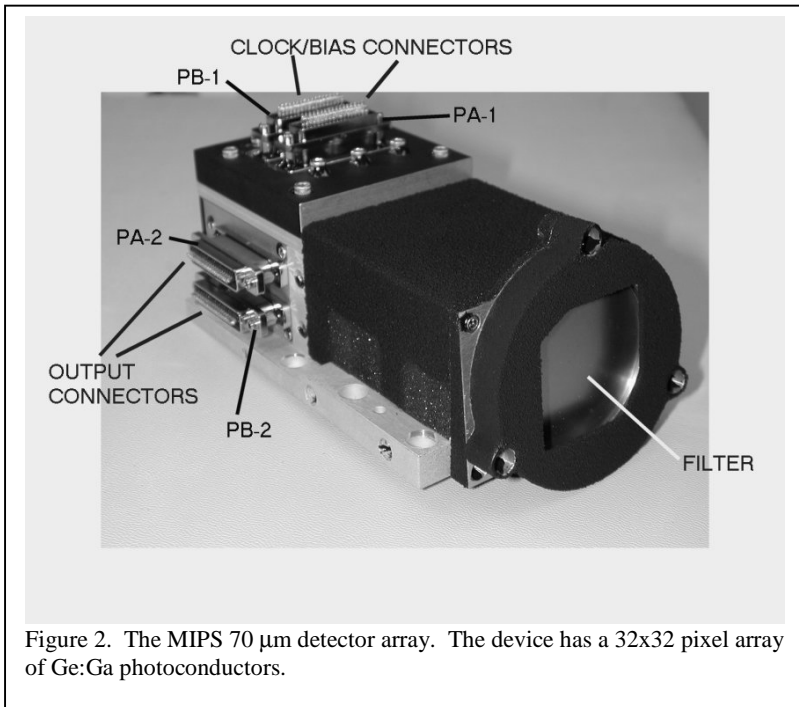


Figure 2. The MIPS 70 μm detector array. The device has a 32x32 pixel array of Ge:Ga photoconductors.

The 70 μm array was developed at the University of Arizona by the MIPS team. The array uses conventional Ge:Ga photoconductors in a 32x32 format and is shown in Figure 2. A number of significant development challenges had to be overcome to produce arrays that met the MIPS performance requirements. Critical was the development of high performance readouts that operated at the low temperatures of the germanium detectors. To meet the dark current requirements, temperatures below 2 K were required for the 70 μm array. Normal silicon circuitry suffers from a number of anomalies at low temperatures⁵, and special features must be incorporated in the design. The MIPS focal plane uses CRC-696 readouts⁶ developed under NASA sponsorship at the Hughes Technology Center (later Raytheon Infrared Center of Excellence). This readout employs a Capacitive Trans-Impedance Amplifier (CTIA) for each pixel. This

circuit is ideal germanium photoconductors because it maintains the detector bias to within a few μV throughout an integration. The design and performance of this array has been discussed by Young et al.⁷

The normal cutoff for Ge:Ga is 115 μm , but the long wavelength response of Ge:Ga photoconductors can be significantly extended by the application of uniaxial stress along the [100] crystal axis.⁸ The required pressure is ~500 MPa, and in the MIPS array design it is applied with a leaf spring made of Aermet 100 high strength steel. The leaf spring provides essentially constant pressure between room temperature and the operating temperature of 1.5 K, and allows the stress to be accurately set during assembly. Additionally, the spring compensates for any relaxation in detector assembly. The actual detector elements are 1 mm cubes of Ge:Ga. Since the photoionization cross section for this material is relatively low, each detector must be placed in an integrating cavity to enhance the absorption efficiency. Feedhorns deliver the infrared radiation to the cavities. The array consists of two rows of 20 pixels, built from four 2x5 modules (see Figure 3). For mechanical reasons, the design requires 1 pixel of space between the detector rows. The 160 μm array uses the same CRC-696 readout as the 70 μm array. Each module has two readouts servicing 5 pixels each. Although the CRC-696 is a 32-channel device, this sparse utilization of the readouts was necessitated by the need to minimize input trace lengths. The design of the stressed array has been described in detail by Schnurr et al.⁹

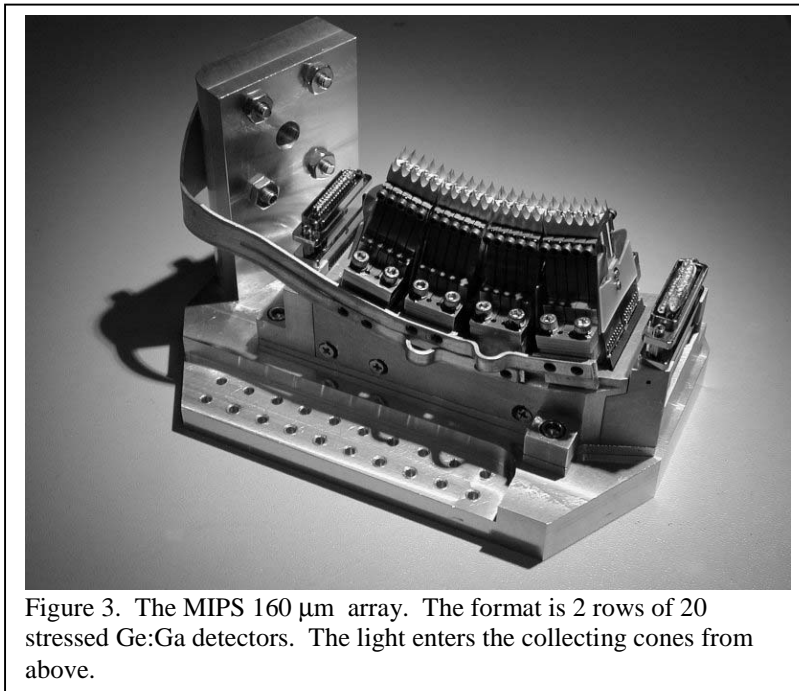


Figure 3. The MIPS 160 μm array. The format is 2 rows of 20 stressed Ge:Ga detectors. The light enters the collecting cones from above.

Each module has two readouts servicing 5 pixels each. Although the CRC-696 is a 32-channel device, this sparse utilization of the readouts was necessitated by the need to minimize input trace lengths. The design of the stressed array has been described in detail by Schnurr et al.⁹

4. SCAN MIRROR AND STIMULATORS

Under very low background conditions, infrared detectors suffer from many non-ideal behaviors. In particular, the conventional photoconductors used in the 70 μm and 160 μm arrays exhibit latent images, multiple time constants, background-dependent time constants, varying responsivity, and radiation effects. The observing philosophy used on MIPS addresses these effects by taking observations in a highly redundant manner, modulating sources in a frequency domain where problems are minimized, and using internal calibrators to continually monitor responsivity. The key subsystems for maintaining the calibration are the scan mirror and the internal stimulators.

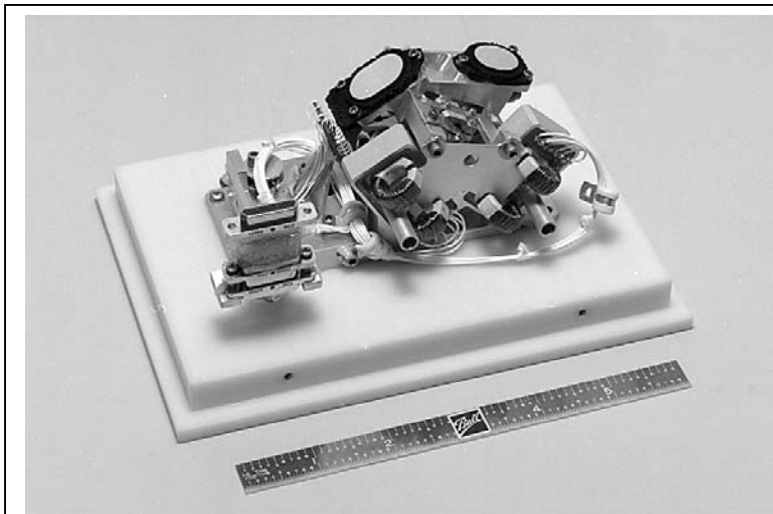


Figure 4. The MIPS Cryogenic Scan Mirror Mechanism.

The Cryogenic Scan Mirror Mechanism (CSMM) is derived from a design used on the Short Wavelength Spectrometer on the Infrared Space Observatory. The ISO design^{10,11} utilizes flex pivots, a voice coil actuator, and a Linear Variable Displacement Transducer (LVDT). To minimize self-heating to optimize the scan mirror for use with the far infrared detectors, a number of changes were made in the design. The copper voice coil actuator was replaced with a niobium-titanium superconducting version. The LVDT was replaced by a differential impedance transducer. These two changes reduced the power dissipation in the device from 1 mW to less than 100 μW . The CSMM has two mirrors mounted on a common carrier and has a total angular range of $\pm 14^\circ$. The CSMM has been described in detail by Warden and Heim.¹² The flight unit is shown in Figure 4.

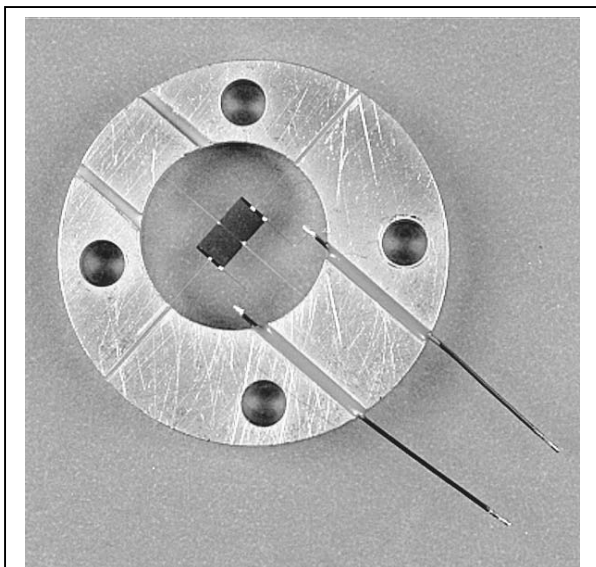


Figure 5. Infrared Stimulator. The emitting area is 2 mm x 4 mm.

Because the responsivity of the detectors changes with time, it is necessary to frequently re-measure this quantity. All the MIPS observing modes adopt this scheme. The functional requirement is for an infrared source that is highly repeatable, has a short time constant, and dissipates very little power. The MIPS stimulators were constructed by Jeffrey Beeman of Lawrence Berkeley Laboratory. The device, shown in Figure 5, is similar in construction to a composite bolometer. A thin sapphire emitting surface is suspended on nylon leads. For the MIPS long wavelength emitters, the substrate size is 2 mm x 4 mm. The sapphire substrate is coated with a thin layer of Nichrome, which acts as a resistive heating element. The thickness of the Nichrome film is designed to give the sapphire substrate a good impedance match to free space and hence results in an efficient emitter. Because the thermal conductivity of the nylon is low, the sapphire rises to a useful temperature with very little power. The low thermal mass of the emitter gives a short time constant. For example, a test stimulator heated to 40 K with less than 2 mW of power dissipation and the associated time constant was less than 1 s. The MIPS observing strategy is to use the stimulators every few minutes to provide very frequent calibrations of the responsivity. Since the anticipated duty cycle is low, the time

average power dissipation will be $< 100 \mu\text{W}$. Based on measurements with bolometer detectors, the repeatability of these stimulators is better than 1%.

5. CHARACTERIZATION FACILITIES

The testing of the MIPS arrays involved testing in a variety of situations depending on the level of integration. Initial characterization was done at the array level in specialized test dewars. Separate dewars were used for the $70 \mu\text{m}$ and $160 \mu\text{m}$ development. Because it would have been difficult to accurately provide both flight-like background levels as well as calibrated sources when looking out a dewar window, we elected to instead use cryogenic sources inside the dewars. We employed both relatively-calibrated stimulators like those used in the flight instrument as well as cryogenic black bodies of our own design. By including a number of independently controlled stimulators we were able to investigate the detector behavior as a function of both background and source brightness.

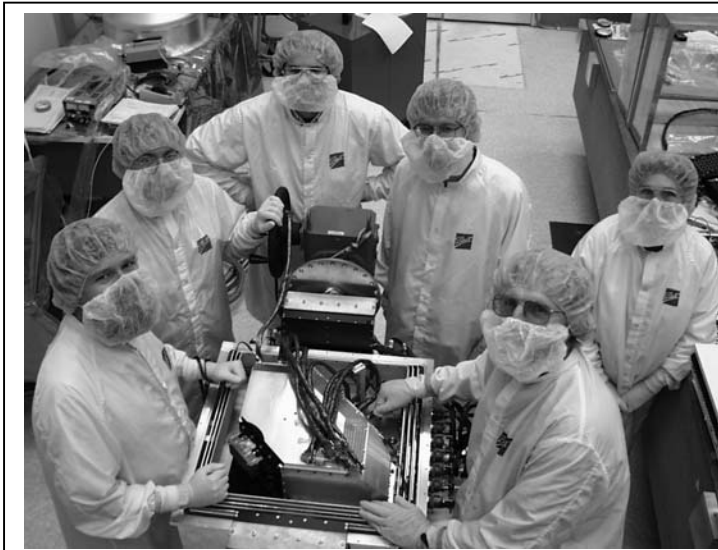


Figure 6. MIPS in the Low Background Test Chamber.

After the detector arrays were installed in the flight MIPS instrument, another, much larger, cryostat was used for instrument level characterization. The instrument mounted in the Low Background Test Chamber (LBTC) is shown in Figure 6. The LBTC was designed to simulate the environment inside the SIRTf instrument chamber, providing extremely low infrared backgrounds and appropriate thermal conditions for the detectors. In particular, the design incorporated multiple radiation shields including ones at 4.2 K, 20 K, and 77 K. A separate heat station cooled with superfluid helium at 1.5 K was used for the detector heat sink. The LBTC has a variety of internal stimulators, point illumination sources, and flood illumination sources needed demonstrate the performance of MIPS. Of particular importance, the LBTC was the only opportunity to measure the imaging performance of the full instrument.

Although some imaging testing at the full observatory level was conducted for the IRAC and IRS instruments using a retroreflecting cryogenic flat, it could not be done for MIPS. The reason for this limitation was that to minimize contamination during ground testing of the observatory, the aperture door on the cryostat could not be opened. The window in the aperture door did not transmit MIPS wavelengths.

At the observatory level, tests have been performed to verify the noise and operability of the MIPS detectors. For these tests, the internal calibration stimulators have been used to provide flood illumination of the arrays. At the observatory level, however, the opportunities for characterization of the array performance are very limited, particularly since the MIPS germanium arrays must be tested at superfluid helium temperatures. In general, the observatory tests are designed to only demonstrate the *functionality* of the instrument under various environmental conditions.

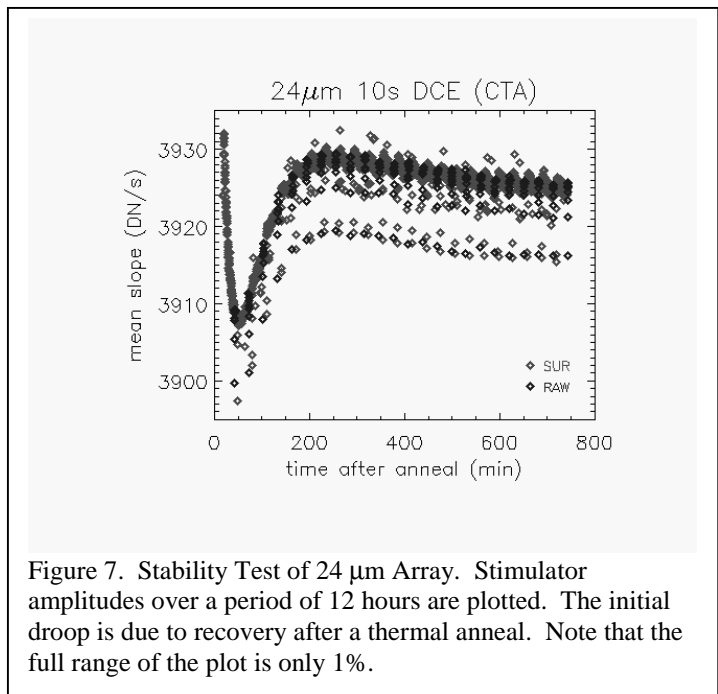
Recognizing that the characterization of the germanium detectors would require significant testing, the MIPS team has constructed two test beds. The test beds feature characterization detector arrays that are as identical as possible to the flight units. In fact, the characterization arrays are built of spare parts from the flight construction effort. These arrays are mounted in dewars that have internal stimulators that can flood illuminate the arrays with a variety of backgrounds and source brightness. The $70 \mu\text{m}$ characterization dewar also includes an off-axis paraboloid to produce an image, and the engineering model CSMM to allow realistic modulation of sources. Both the $70 \mu\text{m}$ and $160 \mu\text{m}$ characterization test sets use flight-like warm electronics. Many of the test results presented in this paper come from the characterization array program.

6- CHARACTERIZATION RESULTS

24 μm Results

The standard operating sequence for the MIPS 24 μm array is to begin an integration with a reset and then to non-destructively read out the array every 0.5 s. The available integration times between resets are 3, 10, and 30 s. Because of limitations in the downlink bandwidth, it is not possible to transmit every frame that is collected by the array. Instead, the instrument computer takes the collection of samples and computes a best-fit slope for each pixel. For a charge integrating amplifier, this slope is proportional to the average photocurrent in each pixel. Additionally, the instrument computer calculates a difference image between the first and second samples. This difference image is useful for recovering photometry of bright sources in the field. Only the difference and slope images are transmitted to the ground. This set of data representing the interval between array resets is termed a Data Collection Event (DCE).

The overall behavior of the 24 μm array is excellent. The read noise, quantum efficiency, and dark current are given in Table 1.



To investigate stability of the array, a considerable amount of data were taken in overnight runs during CTA testing. We collected five nights of 24 μm array data, including two nights with the array under continuous and constant illumination, and three nights with the array in the dark. Each night before data acquisition commenced, a thermal anneal was performed to place the array in a standard configuration. Then, a long series of DCE's were taken, encompassing 12 hrs. Results are plotted in Figure 7. The array mean slope is remarkably constant in each dataset, with variations at only 0.5% or less. The largest variations occur in the first 3 hours or so and likely represent responsivity changes as a result of the thermal anneal. After this initial period, there is a very small downward drift in the slopes, a change of less than 0.2% over 9-10 hours.

The 24 μm arrays does suffer from two undesirable effects. The first effect is called the “droop” effect. The output of each pixel depends not only on the flux falling on that pixel, but also on the total flux falling on the whole array. For the MIPS array, the droop coefficient is 0.32, meaning that 32% of the average integrated charge over the whole array appears on the output of every pixel. We anticipate that the correction software that has been implemented in the calibration pipeline will satisfactorily compensate for the droop effect. The 24 μm array also exhibits long term latent images from bright sources. The decay time is long (~10 minutes). Fortunately, the amplitude of the latent images is small, typically less than 1% of the original source.

70 μm Results

Read Noise and dark current of the flight 70 μm array has been measured at the focal plane level, in the LBTC, and after installation in the Cryo-Telescope Assembly (CTA). The coldest and darkest conditions were realized in the LBTC during instrument testing. Figures 8, 9, and 10 show the dark current, and read noises for 3 and 10 second integration periods. The higher read noise found in the 10-s DCE set can be attributed to excess low frequency noise in the system. The median dark current is

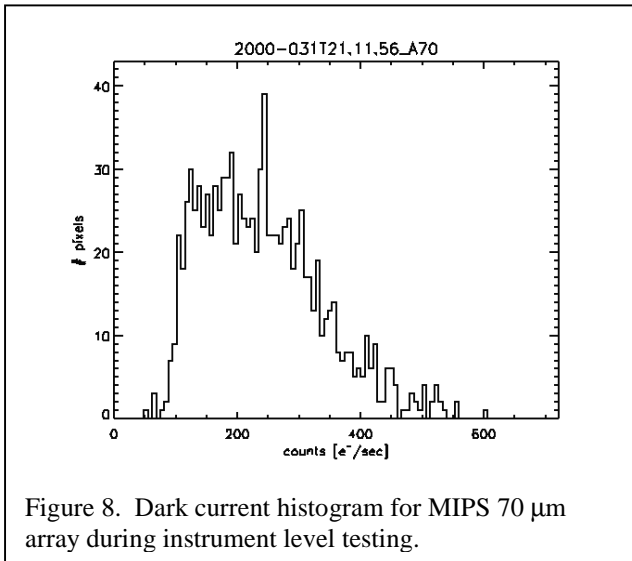


Figure 8. Dark current histogram for MIPS 70 μm array during instrument level testing.

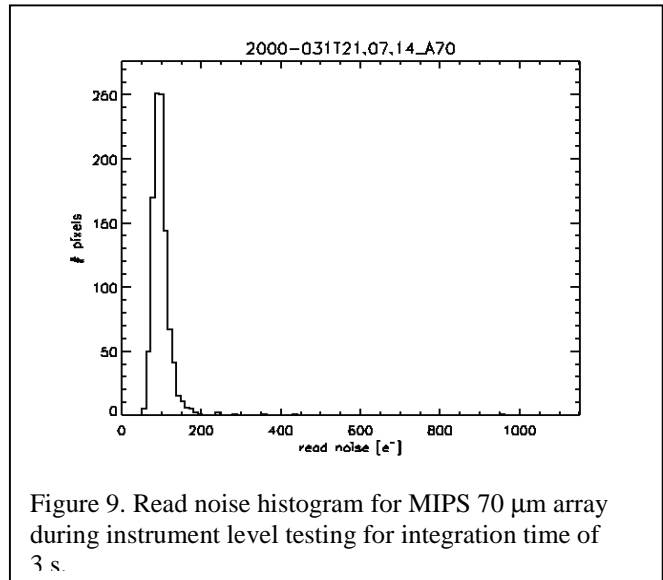


Figure 9. Read noise histogram for MIPS 70 μm array during instrument level testing for integration time of 3 s.

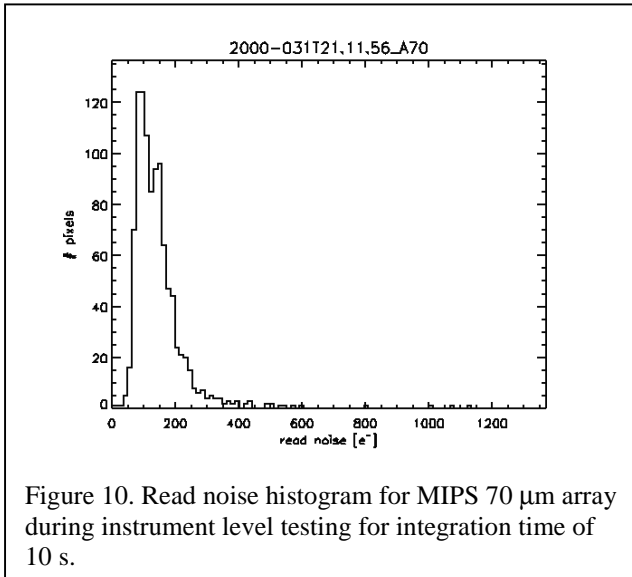


Figure 10. Read noise histogram for MIPS 70 μm array during instrument level testing for integration time of 10 s.

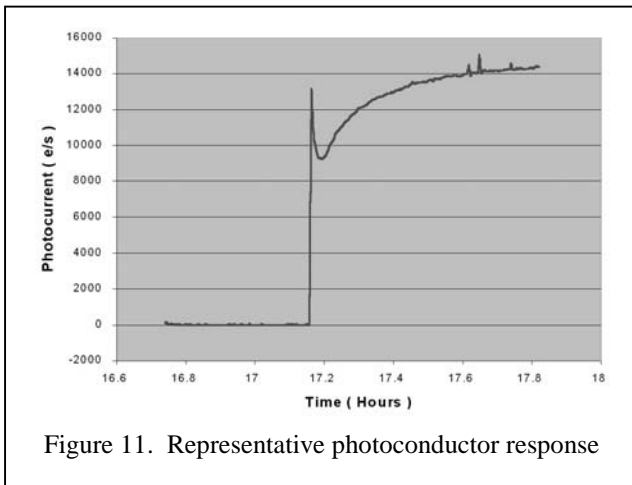


Figure 11. Representative photoconductor response

The responsivity of the 70 μm array was measured in the array test dewar with the aid of an internal black body source. In this system an off-axis parabolic mirror acts as a collimator that flood illuminates the array.

The photometric calibration of conventional photoconductors is complicated by the nonlinear time response of the detector as depicted in Figure 11. Since the MIPS calibration method depends on an accurate calibration of prompt response of the detector, we needed a way to modulate the calibration signal on the appropriate rapid timescale. Rather than introduce a mechanism to modulate the blackbody source, we elected to use a simulator to serve as a secondary calibrator. We determined the current necessary to give the same long-time time constant response as the cryogenic black body, giving us an irradiance vs. current relationship for the stimulator. Pulsing the stimulator then gave us a calibrated irradiance at the desired time scales.

The internal stimulators are also used to correct for the long term response changes that are present in photoconductors. In normal operation, MIPS will take a measurement of an internal stimulator every few minutes. In this way, we are able to track response changes that are due to both non-linearities in the detector as well as changes caused by ionizing radiation in the space environment. Finally, by using the instrument scan mirror to modulate the astronomical sources on a time scale comparable to stimulator flashes, we avoid many of the settling issues associated dielectric relaxation in the detectors.

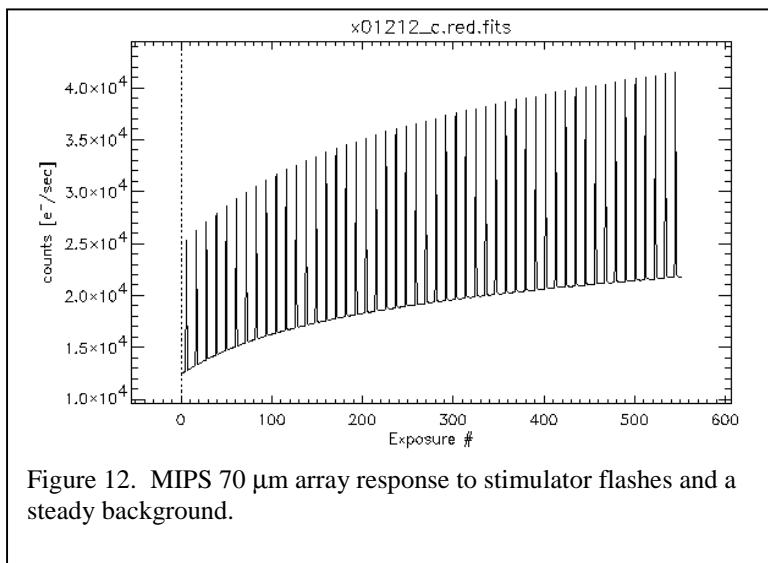


Figure 12. MIPS 70 μm array response to stimulator flashes and a steady background.

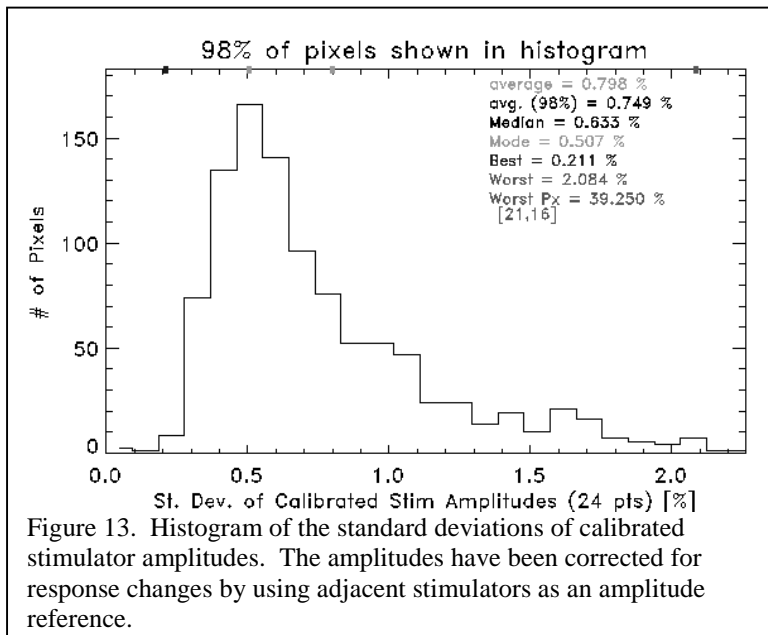


Figure 13. Histogram of the standard deviations of calibrated stimulator amplitudes. The amplitudes have been corrected for response changes by using adjacent stimulators as an amplitude reference.

Figures 12 and 13 illustrate the calibration method. Figure 12 shows the raw response of the 70 μm array to a long series of stimulator flashes on top of a steady background illumination. The entire plot encompasses 6000 seconds of data. As is typical of conventional photoconductors, the response of the array increases with time. This increase is seen in both the background response and the amplitude of the stimulator flashes. Figure 13 shows the repeatability of the odd flash amplitudes if they have been normalized by the even flashes. In this case, the odd flashes would represent astronomical point sources. Despite the large absolute change in response during the course of the run, the calibrated flash amplitudes show excellent repeatability, with a standard deviation of only 0.7% for 98% of the pixels.

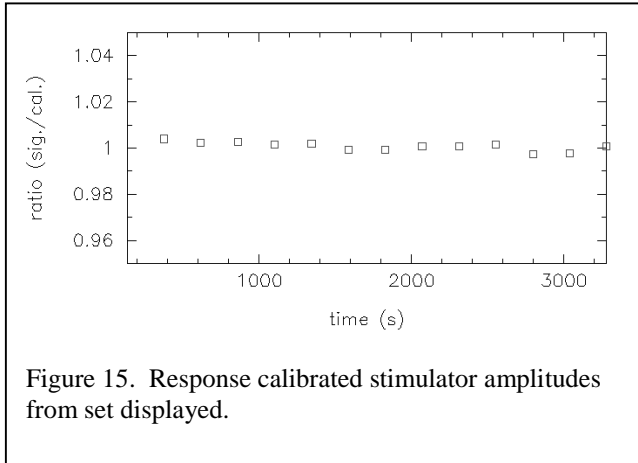
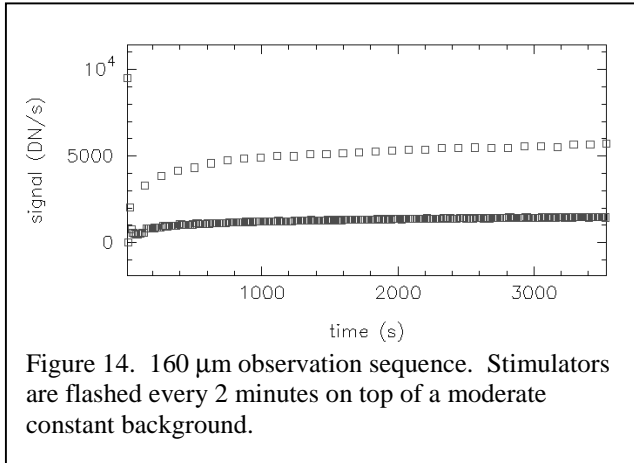
We have investigated image latency effects in the 70 μm array. Most of this investigation has focused on the amplitude of the stimulator latents. The typical latent amplitude is roughly 1% of the amplitude of the stimulator flash and the time constant is in the range 5 - 20 s.

Ionizing radiation can cause significant changes in the responsivity of conventional photoconductors. After exposure, the responsivity can increase by as much as a factor of 10, and this increase slowly decays on a time scale that is background dependent. To avoid the complications in calibrating such behavior, we have included resistive heaters on the focal plane array. By momentarily heating the detectors to ~ 8 K for 10 s, we can restore the responsivity to pre-exposure levels. The anticipated duty cycle for these anneals is small (once per hour), and the total impact on

the power budget is small. The anneal heaters will contribute less than 1mW average power dissipation over the course of the mission. The 70 μm array fully settles within 10 minutes after a thermal anneal.

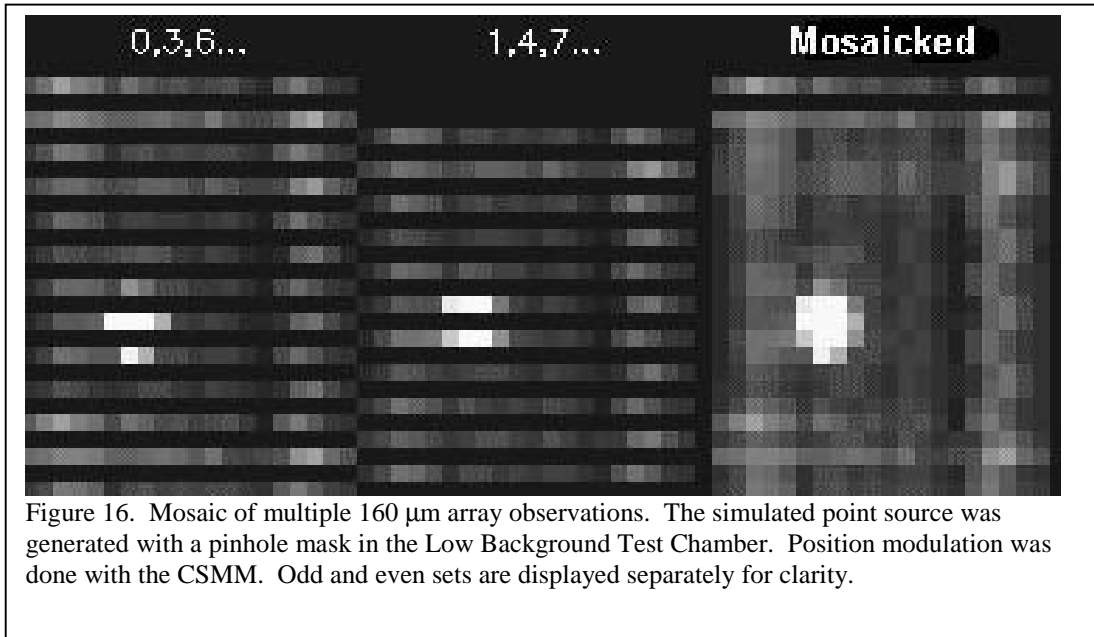
160 micron Results

We utilize a similar calibration strategy for the MIPS 160 μm array. It suffers from the same background-dependent non-linearities as the 70 μm array. Frequent use of the internal stimulators will be used to calibrate these detectors. Figure 14 shows a series of stimulator flashes taken after a thermal anneal. The thermal anneal is used to remove any ionizing radiation effects and to place the array in a known state. Typical anneal conditions are a peak temperature of 4 K and a duration of 10 s. In this example, the array is exposed to a constant, low infrared background, and the stimulators are fired every two minutes. As with the 70 μm array the response to both the stimulators and the background increase as a function of time. Figure 15 shows the result of calibrating the odd flashes with the even



flashes. It is notable that the 160 μm array settles very quickly after the thermal anneal. In a separate test, we have found that the dark current settles to the pre-anneal value in ~ 120 s. Figure 15 shows that the calibration method is quite effective for correcting the responsivity variations of the array. Despite the large change in stimulator and background response during the one-hour run, the calibrated stimulator response is constant to better than 1%.

Because the 160 μm array only has a modest 2×20 pixel format with a gap between the two rows, it will be necessary to build up images by mosaicking multiple observations of regions. The cryogenic scan mirror mechanism (CSMM) will be essential in producing these mosaics efficiently. Figure 16 shows observations of a simulated point source from the Low Background Test Chamber. As can be seen in the combined image, the response and flat fielding accuracy is adequate to properly allow reconstruction of well-sampled point sources.



SUMMARY

The Multiband Imaging Photometer for SIRTf (MIPS) will provide unprecedented astronomical capabilities in the far-infrared. Much of the power of the instrument comes from the advanced detector arrays that will be used in the instrument. We have demonstrated an observational strategy that relies on point source modulation and the frequent use of internal stimulators to provide excellent photometric repeatability.

REFERENCES

-
- ¹ G. B. Heim, M. L. Henderson, K. MacFeely, T. J. McMahon, D. Michika, R. J. Pearson, G. H. Rieke, J. P. Schwenker, D. W. Strecker, C. Thompson, R. M. Warden, D. A. Wilson, and E. T. Young, "Multiband Imaging Photometer for SIRTf," Proc. SPIE, 3356, pp. 985-1000, 1998.
- ² G.G. Fazio, J. L. Hora, S.P. Wilner, J.R. Stauffer, M.L.N. Ashby, Z. Wang, E.V. Tollestrup, J. Pipher, W. Forrest, C. McCreight, S.H. Moseley, W.F. Hoffmann, P. Eisenhardt, E.L. Wright, "The Infrared Array Camera (IRAC) for the Space Infrared Telescope Facility (SIRTf)," Proc. SPIE, 3354, pp. 1024-1031, 1998.
- ³ Thomas L. Roellig, James R. Houck, Jeffrey Van Cleve, Al Rakowski, Chris Stewart, Glenn Taudien, Marty Huisjen, Mary Bolten, and David Seib, "Infrared Spectrograph for the Space Infrared Telescope Facility (SIRTf)", Proc. SPIE, 3354, pp. 1192-1203, 1998.
- ⁴ J. Van Cleve, T. Herter, R. Butturini, G. Gull, J.R. Houck, B. Pirger, and J. Schoenwald, "Evaluation of Si:As and Si:Sb Blocked Impurity Band Detectors for SIRTf and WIRE", Proc. SPIE, 2553, pp. 502-513, 1995.
- ⁵ R.M. Glidden, S.C. Lizotte, J.S. Cable, L.W. Mason, and C. Cao, "Optimization of Cryogenic CMOS Processes for Sub-10 K Applications," Proc. SPIE, 1684, pp. 2-39, 1992.
- ⁶ Erick T. Young, "Progress on Readout Electronics for Far-Infrared Arrays," Proc. SPIE, 2226, pp. 21-28, 1994.
- ⁷ E.T. Young, J.T. Davis, C.L. Thompson, G.H. Rieke, G. Rivlis, R. Schnurr, J. Cadien, L. Davidson, G.S. Winters, and K.A. Kormos, "Far-Infrared Imaging Array for SIRTf," Proc. SPIE, 3354, pp. 57-65, 1998.
- ⁸ A.G. Kazanskii, P.L. Richards, and E.E. Haller, "Far-Infrared Photoconductivity of Uni-Axially Stressed Germanium," App. Phys. Lett., 31, 496, 1977.
- ⁹ R. Schnurr, C.L. Thompson, J.T. Davis, J.W. Beeman, J. Cadien, E.T. Young, E.E. Haller, and G.H. Rieke, "Design of the Stressed Ge:Ga Far Infrared Array for SIRTf", Proc. SPIE, 3354, pp. 322-331, 1998.
- ¹⁰ K.J. Wildeman, D.A. Beintema, G.R. Ploeger, D.Snel, and J.J. Wijnbergen, "Grating Drive for the Short Wavelength Spectrometer in ISO" Cryogenics Vol 27, pp. 68-72, 1987.
- ¹¹ J.W.G Aalders, K.J Wildeman, G.R Ploeger, and Z.N. Van Der Meij, "New Developments with the Cryogenic Grating Drive Mechanisms for the ISO Spectrometers" Cryogenics Vol 29, May, pp. 550-552, 1989
- ¹² Robert M. Warden, Gerald B. Heim, "Cryogenic Scan Mirror Mechanism for SIRTf/MIPS," 32nd Aerospace Mechanisms Symposium, May 1998.